AMERICAN METEOROLOGICAL SOCIETY
AMS Journals Online

Full Text View

A Modeling Study of the Episodic Cross-Frontal Water Transport over the Inner Shelf of the South Atlantic Bight

Changsheng Chen

Department of Marine Sciences, University of Georgia, Athens, Georgia

ABSTRACT

Physical processes that control the episodic cross-frontal transport over the inner shelf of the South Atlantic Bight were examined using a 3D primitive turbulent closure equation model. The model results showed that significant cross-frontal water exchange occurred under upwelling-favorable wind conditions through the detachment of isolated low-salinity lenses at the outer edge of the front. The formation of isolated lenses was a 3D feature associated with complex nonlinear processes. It depended on 1) the amount of multiple river discharges, 2) direction and magnitude of the wind, and 3) tidal mixing. As the total amount of river discharges increased, stronger winds were required to form the isolated lenses. When the river discharges were larger, tidal mixing tended to delay the occurrence of isolated lenses through 1) increasing the cross-shelf gradients of density and surface elevation and thus enhancing the along-shelf current and reducing the along-shelf variation of salinity, and 2) strengthening the internal stress at the bottom edge of the plume and thus slowing down the offshore water transport. The vertical salt diffusion, along-shelf and cross-shelf salt advections played a critical role in the detachment of the low-salinity water from the front. Upwelling significantly contributed to salinity increases near the coastal region in the early wind stages and the lenses' intensification in the midshelf. After the wind subsided, the eddylike circulation developed over the midshelf through adjustment of currents to surface elevation. The residence time of these eddies depended on the initial strength and location of isolated lenses. In the midshelf, where tidal mixing was relatively weak, these eddies could last about one week. In the inner shelf, where the depth was less than 20 m and tidal mixing was stronger, their lifetimes were less than one day.
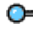
1. Introduction

The inner shelf of the South Atlantic Bight (SAB), bounding at the 20-m isobath, is mainly characterized by a coastal low-salinity frontal zone resulting from the interaction between freshwater discharges, tidal mixing, and wind forcing (Fig. 1). Ten major rivers terminate along the coast of the SAB with a total freshwater discharge of about 1000 $\text{m}^3 \text{ s}^{-1}$ in autumn and 4000 $\text{m}^3 \text{ s}^{-1}$ in spring (Blanton 1981). The maximum discharge exceeds 8000 $\text{m}^3 \text{ s}^{-1}$ during high discharge years like 1984 and 1993 (Blanton 1996). Tidal motion accounts for about 80%–90% (cross shelf) and about 20%–40% (along shelf) of current variation and kinetic energy in the inner shelf of the SAB (Tebeau and Lee 1979; Lee and Brook 1979; Pietrafesa et al. 1985). Tidal current is strongest in the widest part of the shelf between Savannah and Charleston and weakest at the northern and southern ends. The wind varies seasonally, blowing northwestward or northeastward in spring and summer and southeastward or southwestward in winter. In spring, the averaged magnitude of wind speed is about 5 m s^{-1}. However, the maximum wind can exceed 15 m s^{-1} during atmospheric frontal passages. The dynamic system over the

inner shelf of the SAB is mainly controlled by these complex physical processes.

Previous hydrographic measurements taken on the inner shelf of the SAB have revealed the episodic events of cross-frontal, low-salinity water transport under certain meteorological conditions. During spring and summer, when the upwelling-favorable (northeastward) wind prevails over the shelf, some relatively fresh lenses (at least 0.2 psu less than the surrounding water) could form at the outer edge of the low-salinity front (Blanton et al. 1989; Paffenhöfer et al. 1994). These lenses tend to detach from the front and move offshore to the midshelf. Examples of the occurrence of the isolated low-salinity lens can be seen in Fig. 2 ☞, which represents the surface and vertical distributions of salinity off Charleston, South Carolina, as observed during the 1984 pre-Spring Removal Experiment (pre-SPREX: Paffenhöfer et al. 1994). This evidence also was observed in recent hydrographic measurements taken on a cross-shelf transect off Savannah in the spring of 1994 (Nelson and Guarda 1995) and during a regional survey off the South Carolina coast in the summer of 1994 (Moore and Kjerfve 1998). Isolated low-salinity lenses also were revealed by the modeling study of wind-induced water removal from the inner-shelf region of the SAB during spring of 1984 (Kourafalou et al. 1996b).

The physical processes that control the formation of isolated low-salinity lenses in the inner shelf of the SAB have not been well explored. Oey (1986) and Blanton et al. (1989) used a 2D model to examine the response of water currents to surface wind stress. They found that an isolated low-salinity lens could form at the outer edge of the front as a result of wind-induced upwelling. Their model results are consistent with the theory derived from a simple conceptual Ekman model proposed by Csanady (1974). This theory suggests that the response of water currents to upwelling-favorable wind varies from the inner shelf to the middle and outer shelves (Fig. 3 ☞). In the inner shelf, where the water depth is shallow and friction is large, the current responds almost instantaneously to local wind stress. As a result, water moves in the same direction as the wind. In the middle and outer shelves, where the water is deep and friction is weak, the wind-driven current follows an Ekman spiral pattern. An upwelling-favorable wind tends to produce an offshore water transport near the surface and an onshore water transport near the bottom. An isolated low-salinity lens could form as the isopycnals outcrop the surface. This theory also was applied by Chao (1987) to a 3D idealized shelf with a single river discharge. He found that the low-salinity lens could form at the outer edge of the low-salinity plume as a result of wind-induced upwelling. Although the simple conceptual Ekman model, to some extent, can interpret the cause of the formation of isolated low-salinity lenses over the shelf where the wind is a dominant forcing, this theory cannot explain why isolated low-salinity lenses occur only in specific regions of the inner shelf. It is unclear whether this theory also applies to the 3D inner shelf of the SAB where the dynamic system is controlled dominantly by a complex physical process associated with multiple river discharges, tidal mixing, and winds.

Chen et al. (1999) used a 3D primitive equation model to examine the physical processes that control the detachment of low-salinity water from the inner shelf front of the SAB. In spring, under a climatological condition of river discharges and winds, they found that low-salinity water could be episodically removed onto the midshelf through the detachment of isolated low-salinity lenses formed at the outer edge of the front. Such a detachment process happens through two steps. At first, the spatially nonuniform response of current to the upwelling-favorable wind causes a wavelike frontal shape at the outer edge of the frontal zone (Fig. 4 ☞). Then the isolated low-salinity lenses form at the crest, when water on the shoreward side of the crest is displaced by relatively high salinity water advected from the upstream trough south of the crest and diffused upward from the deep region. Wind-induced upwelling does not play a critical role in the formation of isolated lenses under springtime climatological conditions even though it noticeably compensates for water loss due to the offshore near-surface Ekman transport.

The model experiments over the inner shelf of the SAB suggest that the formation of isolated lenses at the outer edge of the low-salinity front is controlled by a 3D physical process associated with along-shelf advection and vertical diffusion. This finding contradicts the traditional Ekman theory in which wind-induced upwelling is a key process controlling the formation of isolated lenses. These numerical experiments also raise a fundamental problem in coastal dynamics in terms of the interaction among river discharges, tides, and winds. Is Chen et al.'s finding a general feature in the inner shelf of the SAB? How does such a 3D wind-induced physical process in the inner shelf of the SAB vary with direction and amplitude of the wind stress and amount of freshwater discharges? Would upwelling become more important in detaching the low-salinity water from the front as winds become stronger? What is the role of tidal mixing in the formation of isolated low-salinity lenses? These questions have not been well explored.

In this paper, I will attempt to address these questions by conducting numerical experiments under different conditions of wind stress (magnitude and direction) and river discharges. To understand the complex interaction processes between multiple river discharges, tides, and winds in the inner shelf, I have conducted numerical experiments that do not include the Gulf Stream. This approach was based on the previous observational results over the SAB, which showed that the Gulf Stream's most significant influences occurred over the outer shelf where the water was deeper than the 60–70-m isobath (Atkinson and Menzel 1985). This study also was conducted with the understanding that neglecting the Gulf Stream might make it impossible to examine the fate of riverine water off the shelf, especially in the region off Charleston where a cyclonic eddy was located (Bane 1983; Singer et al. 1983).

The remaining sections of this paper are organized as follows. In section 2, the design of numerical experiments is described. In section 3, the model results with different magnitudes and directions of winds and river discharges are given. In section 4, the physical processes that control the formation of isolated lenses are examined, and in section 5, the conclusions are made.

2. Design of numerical experiments

The numerical model used in this study is an updated version of the 3D coastal ocean circulation model originally developed by Blumberg and Mellor (1987) (called ECOM-si). This is a fully nonlinear, prognostic model incorporating the free surface and the Mellor and Yamada (1974, 1982) level-2.5 turbulent closure scheme for vertical mixing. Unlike the original Blumberg and Mellor (1987) time-splitting model (called POM), the updated version of the ECOM-si incorporates a semi-implicit scheme in the horizontal for the barotropic mode calculation. It treats both the barotropic pressure gradient in the momentum equations and the velocity convergence in the continuity equation implicitly. This method leads to a linear

symmetrical diagonal system at each time step, which can be solved efficiently by a preconditioned conjugate method with no sacrifice in computational time (Casulli 1990; Chen and Beardsley 1995, 1998). The governing equations and boundary conditions as well as tidal simulation were given and discussed in Chen et al. (1999). A brief description is provided here.

The model domain covered the entire shelf region bounded at Cape Hatteras, North Carolina, to the north and at Cape Canaveral, Florida, to the south. The offshore open boundary was specified using a curved line parallel to the local isobath with a maximum depth cutoff of 600 m. Horizontal resolution was 1.5 km in the cross-shelf direction and 2 km in the along-shelf direction in the inner shelf and about 15 km close to the offshore open boundary. A σ-coordinate transformation (31 levels) was used in the vertical, which corresponded to a vertical resolution of about 0.1 m near the coast and 20 m at the 600-m isobath. The time step used in our experiments was 931.5 seconds.

The model was forced initially by the oscillating M_2 tide at open boundaries. The sea level data used for tidal forcing were adopted directly from the global $0.5° \times 0.5°$ tidal model developed recently by Egbert et al. (1994). To simplify the model problem and focus on the physical processes that control the formation of isolated low-salinity lenses in the inner shelf of the SAB, I ignored the spatial structure of the background temperature by taking a constant value of 20°C. I also assumed that the initial background salinity was a constant value of 35 psu everywhere in the model domain. This assumption was consistent with our understanding that any spatial variation of water salinity in the inner shelf developed as a result of multiple river discharges, wind, and tidal mixing.
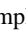
After tidal currents reached a quasi-equilibrium state, freshwater was injected into the model domain at coastal boundaries from ten river sources. To examine the influence of river discharges on the formation of isolated low-salinity lenses, I first ran the model using the river discharge rates averaged over 7 to 74 years (indicated as R_m), and then increased the freshwater flux to be α times as large as R_m, where α varied from 1 to 5 (corresponding to the range of the total discharge rate from 2060 to 10 300 m^3 s^{-1}). I also ran the model for an idealized case with a uniform discharge from five major rivers. Comparison of the model results between uniform and spatial-varying river discharges provided us some insights into the effects of the along-coastal variation of river discharge on the cross-frontal detachment of low-salinity water in the inner shelf.
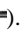
To understand the wind's role in this inner-shelf system, I ran the model first for constant wind speeds and directions and then for varying winds. In these cases, the wind was added at the 100th model day as the low-salinity front in the central region of the inner shelf of the SAB reached a quasi-equilibrium state. The wind also was added at the 10th, 50th, and 80th model days during a developmental period of the front to examine the degree to which the occurrence of isolated low-salinity lenses relied on the total amount of the river water in the inner shelf.

3. Model results

a. The constant wind case

The numerical experiments showed that the formation of isolated low-salinity lenses (defined as the closed salinity contours that are at least 0.2 psu fresher than the surrounding water) in the inner shelf of the SAB was closely related to river discharge rates, wind speeds and directions, and tidal mixing. In the case with a total discharge rate of $3R_m$ (6180 m^3 s^{-1}), for example, isolated low-salinity lenses occurred under an upwelling-favorable (northeastward) wind condition only when the wind speed was equal to or greater than 6 m s^{-1} (Fig. 5 ⊙). The shapes and intensities of these lenses also varied with wind speed. In the case with a wind speed of 8 m s^{-1}, two well-defined low-salinity lenses were observed near the Pee Dee and Altamaha Rivers 5 days after the wind blew. The sizes of these two lenses became larger as they were advected offshore and mixed with the surrounding water. As the wind speed increased to 10 m s^{-1}, a well-defined isolated low-salinity lens occurred on the second day near the Altamaha River, about 3 days earlier than that in the 8 m s^{-1} wind case. This isolated lens became much larger in size and fresher in successive days as it was advected offshore onto the midshelf. An isolated lens also was observed near the Pee Dee River in this case. The size of that lens, however, was much smaller because of stronger wind mixing.

The model results showed that isolated low-salinity lenses occurred only in cases with an upwelling-favorable wind condition (see Fig. 6 ⊙ for example). The downwelling-favorable wind tended to intensify the low-salinity front by increasing the onshore Ekman transport near the surface and thus reinforced a southward along-shelf water transport. Similar results also were true for off- and onshore winds, where water tended to be advected southward (offshore wind) or northward (onshore wind) along the coast by the wind-induced Ekman transport. These features, in general, remained unchanged with wind speeds in both cases with or without inclusion of the M_2 tide. These findings also were consistent with previous studies done over idealized shelves (Chao 1987, 1988; Kourafalou et al. 1996a)

An exception may occur for a large river discharge in which the low-salinity water converges and then moves offshore in the northern region of Florida where the coastline bends and extends southeastward (Fig. 7, left panel ⊙). The offshore detachment of the low-salinity water around the "bent" coastal region in northern Florida was evident during the high discharge year of 1984. The satellite coastal zone color scanner (CZCS) picture taken on 4 March 1984 showed a relatively high area of phytoplankton pigment concentration in the midshelf around 30.5°N (Fig. 7, right panel ⊙). This was in good agreement in terms of location with the offshore detachment of low-salinity water shown in Fig. 7 ⊙. The seaward removal of low-salinity water in this area was caused by a downstream accumulation of water through a convergent current along the coast, as suggested by the laboratory and numerical model experiments over an idealized shelf by Stern et al. (1982) and Chao (1988).

Isolated low-salinity lenses can form in the case with no tidal forcing. An example is given in Fig. 8 ⊙ for the case with a

total discharge rate of $3R_m$. For a given wind speed of 8 m s^{-1}, the well-defined isolated low-salinity lenses formed on the second model day after the wind blew. These lenses became larger and fresher as they migrated offshore in successive days. Compared with the case with tidal forcing, the intensities of the lenses in this case were weaker and also it took a shorter time for them to form. Similar features can be also seen in the case with a constant wind of 10 m s^{-1}.

The relationship between the formation of isolated low-salinity lenses and river discharges, upwelling-favorable winds, and tidal mixing is examined next. In the case without tidal forcing, the occurrence of isolated lenses was controlled mainly by wind speed rather than river discharge (Fig. 9a ⊙). No formation of lenses was found when the wind was weaker than 5.5 m s^{-1}. When tidal forcing was included, the formation of isolated lenses relied closely on both wind speed and river discharges. As the total river discharge rate increased, a stronger wind was required to form the isolated lenses (Fig. 9b ⊙). In the case with a river discharge rate R_m, the minimum wind required for the formation of isolated lenses was 5 m s^{-1}. When the discharge rate increased to $5R_m$, a minimum wind speed of 7.5 m s^{-1} was needed.

The time required to form the isolated low-salinity lenses changed with the river discharge rate, wind speed, and tidal mixing. In the case without tidal forcing, for a given upwelling-favorable wind, the time required for the formation of isolated lenses was generally shorter as the total river discharge rate became larger (Fig. 10a ⊙). As the wind became stronger, the time required to form isolated lenses became shorter, and when the wind reached a certain level, the occurrence times of isolated lenses became closer. For a given wind speed of 6 m s^{-1}, for example, it took about 5 days to form isolated lenses in the case with the total river discharge rate of $3R_m$, while it only took about 3.5 days when the river discharge rate increased to $5R_m$. The time difference between these two cases was less than half a day when the wind increased to 10 m s^{-1}. No significant time difference was observed when the river discharge rate was larger than $4R_m$ and the wind was stronger than 7 m s^{-1}.

In general, tidal mixing tended to delay the occurrence of isolated lenses. For example, in the case with a total river discharge rate of $3R_m$, it took about 2 or 3 more days to form isolated lenses in a case with tide than in a case without tide (Fig. 10b ⊙). In the case without tide, a wavelike shape of the salinity front developed rapidly, and then isolated lenses occurred on the second wind day as a result of detachment of low-salinity water from the front (Fig. 11 ⊙, left panel). In the case with tide, however, tidal mixing tended to reduce the along-shelf variation of salinity and thus slowed the formation of the wavelike shape of the salinity front near rivers (Fig. 11 ⊙, right panel). An analysis of cross- and along-shelf momentum balances indicated that the wind-induced Ekman flow only accounted for one-third of the water transport in the low-salinity plume. Tidal currents enhanced vertical mixing near the coast and hence strengthened the cross-shelf gradients of density and surface elevation. As a result, the along-shelf current was significantly accelerated, which tended to reduce the along-shelf variation of salinity. In both cases with and without tide, the internal stress at the bottom edge of the plume always acted like a drag force to retain or deaccelerate the offshore water transport. This drag force tended to be strengthened in the case with tide, which directly slowed down the offshore water movement. The delay in occurrence of isolated lenses was a result of the tide-induced increase of cross-shelf pressure gradients and internal stress.

This finding, however, was only true for the larger river discharge cases ($>R_m$). In a weak discharge case ($\sim R_m$) without tidal forcing, the isolated lenses only occurred when the wind speed was equal to or stronger than 6.5 m s^{-1}. In the case with tidal forcing, lenses can appear under a weaker wind of 5 m s^{-1} (Fig. 9 ⊙). As pointed out by Chen et al. (1999), in a weak discharge case, tidal mixing tended to enhance the momentum transfer in the vertical, which produced a relatively weak wind-driven current at the surface. The combined current vector of river discharge and wind shifted significantly offshore near rivers, forming a wavelike shape of the low-salinity front as shown in Fig. 4 ⊙. This would not happen in the case without tidal forcing, where the combined current vector of river discharges and wind was dominated by the wind-induced current, which was mainly limited to a thin layer near the surface and was relatively uniform over the shelf.

All findings discussed above were based on numerical experiments in which the wind was added after the low-salinity front in the center of the inner shelf of the SAB reached a quasi-equilibrium state by the 100th model day. Does the occurrence of isolated low-salinity lenses also depend on the total amount of the freshwater injected onto the shelf? To address this question, I ran the model by adding wind forcing at the 10th, 50th, and 80th model days before the quasi-equilibrium state of the low-salinity front was reached. An example of the model results for the case with a constant wind of 8 m s^{-1} and a total river discharge rate of $3R_m$ is shown in Fig. 12 ⊙.

The model showed the occurrence of isolated low-salinity lenses in all three cases. This suggests that the occurrence of these lenses did not depend on the total amount of the freshwater injected onto the shelf. On the other hand, the time required for the formation of these isolated low-salinity lenses did vary with the total amount of freshwater. It took less time in the case where the wind started at the 10th model day and a little longer in the case where the wind started at the 50th and 80th days. The shape, intensity, and spatial distributions of these lenses also depended on the total amount of the freshwater. The lenses were much fresher in the case with the greater amounts of freshwater.

b. The variable wind case

Generally speaking, the near-surface wind field over the SAB in spring and summer was dominated by a subtropic anticyclone with high pressure east of Florida. This large-scale high pressure atmospheric system produced a southwesterly wind over the inner shelf of the SAB. The synoptic-scale wind field, however, was intermittently altered by atmospheric frontal passages with a timescale of about 5 to 7 days (Weber and Blanton 1980). To examine the effects of the variable wind field on the formation of isolated low-salinity lenses in the inner shelf of the SAB, I conducted several numerical experiments with a variable southwesterly wind. Examples are presented in Figs. 13 ⊙ and 14 ⊙, in which the wind speed

was given as a step function in the form of

$$W_s = \begin{cases} 10 \text{ m s}^{-1}, & 0 \le t \le 5 \text{ days} \\ 0, & 5 < t < 10 \text{ days} \\ 10 \text{ m s}^{-1}, & 10 \le t \le 15 \text{ days}, \end{cases}$$

where t was the time that started counting as the wind forcing was added.

Isolated low-salinity lenses formed on the second day after the wind blew. These lenses intensified as they were advected offshore and completely detached from the low-salinity front on the fourth successive day. When the wind relaxed after the fifth day, the current adjusted rapidly to the density field associated with the low-salinity front in the inner shelf and isolated low-salinity lenses in the midshelf within an inertial period. Isolated low-salinity lenses tended to become larger in size and gradually were diffused as they migrated offshore. When the wind started blowing again, the new isolated low-salinity lenses formed on the 12th day, just two days after the wind began. Although the shape and location of the isolated low-salinity lenses differed slightly from those found in the first wind event, the time required for the formation of these lenses remained almost unchanged. This suggests that cross-frontal water exchanges can occur episodically through the detachment of low-salinity water lenses in the inner shelf of the SAB during the atmospheric frontal passages in spring and summer.

c. The uniform river discharge case

To examine the effects of river discharge spatial variation on the formation and evolution of isolated low-salinity lenses associated with the low-salinity front in a multiple river system, I ran the model for the case with uniform river discharge. Five major rivers (Cape Fear, Pee Dee, Cooper, Savannah, and Altamaha Rivers) were considered in this experiment. The discharge rate for each river was specified as $0.6R_m$, with an average value of $3R_m$ for the five rivers. In order to make a comparison with the constant wind case, the wind was added into the model as the low-salinity front reached a quasi-equilibrium state by the 100th model day. In the case with a constant wind speed of 10 m s^{-1}, for example, the well-defined isolated low-salinity lenses occurred at the outer edge of the low-salinity front 2 days after the wind began (Fig. 15 ◯▬). As these lenses moved offshore, they expanded in the along-shelf direction and formed a relatively low-salinity zone in the middle shelf north of the Savannah River. Near the Altamaha River, where the curvature of the coastline was largest, the occurrence of a less saline lens in the middle shelf was the result of wind plus a southward convergence of low-salinity water.

This model experiment suggests that the existence of multiple isolated low-salinity lenses in the midshelf during the southwesterly wind was closely related to the difference in the freshwater discharge from rivers and the curvature of the local coastline. In the case with a uniform river discharge, multiple isolated low-salinity lenses were observed in a certain time interval during an upwelling-favorable wind, but they eventually merged into a relatively uniform low-salinity zone in the midshelf. The model experiments also have revealed that the time required for the formation of this uniform zone depended on the distance between rivers, freshwater discharge rate, and wind speed.

d. The relaxation of the wind

When an upwelling-favorable wind blew northeastward along the coast, the water current responded immediately and formed a northeastward flow near the surface over the entire inner shelf (Fig. 16a ◯▬). The isolated lens that formed during the wind event was just a passive salinity feature that had no similarity to eddies. After the wind subsided or ceased, the current quickly adjusted to the salinity field and surface elevation within a local inertial timescale. Over the inner shelf, a southward residual current reappeared within the low-salinity frontal zone, while an eddylike circulation developed in the isolated lens as a result of the adjustment of the current to the surface elevation (Figs. 16b–d ◯▬ and 17b–d ◯▬). The residence time of eddies depended on the initial locations and intensities of isolated lenses. In the midshelf, where tidal mixing was relatively weak, these eddies stayed for about one week. In the inner shelf, where the water was less than 20 m, they lasted less than a day because of strong tidal mixing.

4. Mechanism study

Three fundamental questions are raised here: 1) What causes the along-shelf variation of the local offshore water transport under an upwelling-favorable wind over the inner shelf of the SAB? 2) What physical processes are responsible for the detachment of low-salinity water from the inner-shelf front? 3) Do these processes differ under various conditions of river discharges and wind forcings? Chen et al. (1999) explored the physical mechanism for the formation of isolated low-salinity lenses in the inner shelf of the SAB. Under a climatological condition of upwelling-favorable wind and a weak river discharge, they found that isolated low-salinity lenses could formed episodically in two steps. At first, a wavelike frontal shape developed at the outer edge of the frontal zone. Then the isolated low-salinity lenses formed at the crest when water at the shoreward side of the crest was displaced by relatively high salinity water advected northward from the upstream trough and diffused vertically from the deeper region. The wavelike shape of the low-salinity front was caused by the combined effects of wind and river discharge, which tended to cause the divergence and convergence zones on the northern and southern sides of rivers. The along-shelf divergence and convergence zones led to a northward decrease of the surface elevation in the along-shelf direction and hence caused a significant offshore low-salinity water transport near larger discharge rivers. Are the Chen et al. (1999) findings still valid in the case with larger river discharges and stronger winds? This question is addressed next.

To examine the along-shelf variation of the offshore water transport under an upwelling-favorable wind, I conducted a diagnostic analysis of the along- and cross-shelf momentum equations. Since tidal mixing generally was not a critical process in the formation of isolated lenses, we can simplify our mechanism study to the case without tidal forcing. In order

to make comparisons with the weak discharge case described in Chen et al. (1999), our analysis here focuses on the case with a large discharge case.

Figure 18 ⊙ shows the cross-shelf distributions of each term in the cross-shelf momentum equation integrated over the upper 5 m on sections 1 and 2 (indicated in Fig. 11 ⊙) for the case with a large discharge of $3R_m$ and a constant southwesterly wind of 8 m s^{-1}. During the first 2 hours after the wind began, the response of cross-shelf water transport to the wind was relatively uniform on these two sections, except in the inner-shelf region where it decreased toward the coast. The along-shelf convergence zone that existed between sections 1 and 2 was the result of the along-shelf variation in the along-shelf current. A significant along-shelf variation of the cross-shelf water transport occurred within a region 20–35 km away from the coast. This was caused by a complex nonlinear process associated with vertical diffusion, cross-shelf, along-shelf, and vertical advections, cross-shelf gradients of surface elevation and density, and Coriolis deflection. A sharp peak in the local change of the cross-shelf water transport was found in the midshelf. It was caused mainly by the vertical and cross-shelf advections. The temporal variation of the cross-shelf water transport significantly decreased 1.5 days after the offshore detachment of the low-salinity water. At that time, the cross-shelf momentum balance was among vertical diffusion, the cross-shelf gradient of the surface elevation and density, and the Coriolis force within the low-salinity plume near the coast. Offshore of the front, the balance was between the cross-shelf gradient of the surface elevation and the Coriolis force offshore from the front.

This result suggested that the cause of the along-shelf variation of the offshore water transport in the case with a larger river discharge rate and a strong upwelling-favorable wind was much more complex than that proposed by Chen et al. (1999) for a climatological condition of upwelling-favorable wind and a weak river discharge. The response of the current to the wind was mainly controlled by a linear process in a weak river discharge case but by a full nonlinear process in a larger river discharge case.

The physical mechanism responsible for the formation of isolated lenses at the outer edge of the low-salinity front is discussed next. In the case of a large river discharge of $3R_m$, for example, an increase in the offshore water transport directly caused a decrease in salinity over the inner shelf during the first day after the wind began (Fig. 19 ⊙). The along-shelf variation of this transport caused the water at the outer edge of the front to be fresher on section 2 than on section 1. Along-shelf advection and upwelling plus vertical diffusion, which developed 6 hours after the wind blew, directly contributed to an increase of salinity in the inner shelf around 10 km away from the coast. Vertical salt advection, however, decreased rapidly one day after the wind began, and the continuous increase in salinity near the coast was driven dominantly by vertical salt diffusion and along-shelf salt advection against cross-shelf salt advection. The isolated low-salinity lens formed 1.5 hour later, when water at the shoreward side of the crest of the front (15–20 km away from the coast) was displaced by relatively high salinity water advected from the downstream trough (along-shelf salt advection), inner shelf (cross-shelf salt advection), and diffused vertically from the deeper region. The relatively high-salinity water, which was advected offshore during this process, was caused by upwelling plus along-shelf salt advection in the early wind stage and by along-shelf advection plus vertical diffusion later. Although upwelling appeared to make no significant contribution to the detachment of the low-salinity water at the outer edge of the front, it became dominant in the intensification of isolated low-salinity lenses as they were advected to the midshelf.

This result implied that the formation of isolated low-salinity lenses over the inner shelf of the SAB was a 3D feature that was caused by much more complex physical processes than those described in a simple wind-induced Ekman theory. These processes varied with wind speed and river discharges. As river discharges and wind speed increased, the offshore salt advection appeared to become an important factor in the formation of low-salinity lenses in the inner shelf of the SAB.

5. Conclusions

Physical processes that control the formation of isolated low-salinity lenses at the outer edge of the low-salinity front over the inner shelf of the SAB were examined using a fully three-dimensional SAB model (Chen et al. 1999). Process studies were conducted by running the model under different river discharge rates and winds with and without tidal forcing. The model results show that isolated low-salinity lenses can form only under upwelling-favorable wind conditions. These lenses occurred episodically in two steps. At first, an increase of the near-surface, offshore water transport near rivers led to the formation of a wavelike frontal shape at the outer edge of the inner-shelf frontal zone. This process was driven dominantly by a linear barotropic process in a weak discharge case but by a complex nonlinear process in a larger discharge case. The isolated low-salinity lenses, then, formed at the crest as water at the shoreward side of the crest was displaced by relatively high salinity water advected from the downstream trough (through the along-shelf salt advection), inner shelf (through the cross-shelf salt advection), and diffused upward from the deeper region. Upwelling made a significant contribution to the increase in salinity near the coastal region during the early wind stage and the intensification of isolated lenses in the midshelf.

The formation of isolated lenses depended on 1) the amount of multiple river discharges, 2) the direction and magnitude of the wind, and 3) tidal mixing. In the case of springtime climatologically averaged river discharges and winds, isolated lenses formed only when the wind was greater than 5 m s^{-1} in the inner shelf of the SAB. A stronger wind was required to form isolated lenses as the total amount of river discharges increased. When the river discharges were larger, tidal mixing acted like a drag forcing to delay the occurrence of isolated lenses. Isolated low-salinity lenses also can form in cases without tidal forcing. The spatial structures of these lenses were significantly different between the cases with and without tidal forcing.

Isolated lenses over the inner shelf of the SAB were simply wind-induced passive salinity features, which were significantly distinct from eddies. After the wind subsided or ceased, the current quickly adjusted to the salinity field and surface elevation. An eddylike circulation developed in the isolated lens as a result of the adjustment of current to surface elevation. The residence time of eddies was relative to the initial locations of these isolated lenses prior to the cessation of the wind. In the midshelf, where tidal mixing is relatively weak, these eddies can last about one week. In the inner shelf region, where the water depth was less than 20 m, they lasted less than one day because of strong tidal mixing.

In the cases with a large river discharge and a strong wind, tidal mixing tended to delay the occurrence of isolated lenses. In these cases, the wind-induced Ekman flow only accounted for one-third of the water transport in the low-salinity plume. Tidal currents tended to enhance vertical mixing and strengthened the cross-shelf gradients of density and surface elevation. As a result, the along-shelf current was accelerated, which tended to reduce the along-shelf variation of salinity. In both cases with and without tide, the internal stress at the bottom edge of the plume always acted like a drag force to retain or de-accelerate the offshore water transport. This drag force tended to be strengthened in the case with tide, which directly slowed down the offshore water transport. The delay in the occurrence of isolated lenses was a result of the tide-induced increase of cross-shelf pressure gradients and internal stress.

REFERENCES

Atkinson, L. P., and D. W. Menzel, 1985: Introduction: Oceanography of the southeastern United States continental shelf. *Oceanography of the Southeastern U.S. Continental Shelf,* L. P. Atkinson, S. W. Menzel, and K. A. Bush, Eds., Coastal and Estuarine Sciences, Vol. 2, Amer. Geophys. Union, 1–9..

Bane, J. M., 1983: Initial observations of the surface structure and short-term variability of the seaward deflection of the Gulf of Stream off Charleston, SC. *J. Geophys. Res.,* **88,** 4673–4684..

Blanton, J. O., 1981: Ocean currents along a nearshore frontal zone on the continental shelf of the southeastern United States. *J. Phys. Oceanogr.,* **11,** 1627–1637.. Find this article online

——, 1996: Reinforcement of gravitational circulation by wind. *Buoyancy Effects on Coastal and Estuarine Dynamics,* Coastal and Estuarine Studies, Vol. 35, Amer. Geophys. Union, 47–58..

——, L. Y. Oey, J. Amft, and T. N. Lee, 1989: Advection of momentum and buoyancy in a coastal frontal zone. *J. Phys. Oceanogr.,* **19,** 98–115.. Find this article online

Blanton, J., F. Werner, C. Kim, L. Atkinson, T. Lee, and D. Savidge, 1994: Transport and fate of low-density water in a coastal frontal zone. *Contin. Shelf Res.,* **14,** 401–427..

Blumberg, A. F., 1994: A primer for ECON-si. Tech. Rep., HydroQual, Inc., Mahwah, NJ, 66 pp. [Available from HydroQual, Inc., 1 Lethbridge Plaza, Mahwah, NJ 07430.].

Blumberg, A. F., and G. L. Mellor, 1987: A description of a three-dimensional coastal ocean circulation model. *Three-Dimensional Coastal Models,* N. S. Neap, Ed., Coastal and Estuarine Sciences, Vol. 4, Amer. Geophys. Union, 1–16..

Casulli, V., 1990: Semi-implicit finite-difference methods for the two-dimensional shallow water equations. *J. Comput. Phys.,* **86,** 56–74..

Chao, S. Y., 1987: Wind-induced motion near the inner shelf fronts. *J. Geophys. Res.,* **92,** 3849–3860..

——, 1988: Wind-driven motion of estuarine plumes. *J. Phys. Oceanogr.,* **18,** 1144–1166.. Find this article online

Chen, C., and R. C. Beardsley, 1995: A numerical study of stratified tidal rectification over finite-amplitude banks. Part I: Symmetric bank. *J. Phys. Oceanogr.,* **25,** 2090–2110.. Find this article online

——, and ——, 1998: Tidal mixing and cross-frontal particle exchange over a finite amplitude asymmetric bank: A model study with application to Georges Bank. *J. Mar. Res.,* **56,** 1163–1201..

——, L. Zheng, and J. O. Blanton, 1999: Physical processes controlling the formation, evolution, and perturbation of the low-salinity front in the inner shelf off the southeastern U.S.: A modeling study. *J. Geophys. Res.,* **104,** 1259–1288..

Csanady, G. T., 1974: Barotropic current over the continental shelf. *J. Phys. Oceanogr.,* **4,** 357–371.. Find this article online

Egbert, G. D., A. F. Bennett, and M. G. G. Foreman, 1994: TOPEX/POSEIDON tides estimated using a global inverse model. *J. Geophys. Res.,* **99,** 24 821–24 852..

Kourafalou, V. H., L. Y. Oey, J. D. Wang, and T. N. Lee, 1996a: The fate of river discharge on the continental shelf. 1. Modeling the river plume and the inner shelf coastal current. *J. Geophys. Res.,* **101,** 3415–3434..

——, T. N. Lee, L. Y. Oey, and J. D. Wang, 1996b: The fate of river discharge on the continental shelf: 2. Transport of coastal low-salinity water under realistic wind and tidal forcing. *J. Geophys. Res.,* **101,** 3435–3455..

Lee, T. N., and D. Brook, 1979: Initial observations of current, temperature and coastal sea level response to atmospheric and Gulf Stream forcing. *Geophys. Res. Lett.,* **6,** 321–324..

Mellor, G. L., and T. Yamada, 1974: A hierarchy of turbulence closure models for planetary boundary layers. *J. Atmos. Sci.,* **31,** 1791–

1806.. Find this article online

— , and — , 1982: Development of a turbulence closure models for geophysical fluid problem. *Rev. Geophys. Space Phys.,* **20,** 851–875..

Moore, W. S., and B. Kjerfve, 1998: Identification of rain-freshened plumes in the coastal ocean using Ra isotopes and Si. *J. Geophys. Res.,* **103** (C4), 7709–7717..

Nelson, J. R., and S. Guarda, 1995: Particulate and dissolved spectral absorption on the continental shelf of the southeastern United States. *J. Geophys. Res.,* **100,** 8715–8732..

Oey, L. Y., 1986: The formation and maintenance of density fronts on the U.S. southeastern continental shelf during winter. *J. Phys. Oceanogr.,* **16,** 1121–1135.. Find this article online

Paffenhöfer, G. A., L. P. Atkinson, T. N. Lee, J. O. Blanton, B. K. Sherman, and T. B. Stewart, 1994: Variability of particulate matter and abundant zooplankton off the southeastern United States during spring of 1984 and 1985. *Contin. Shelf. Res.,* **14,** 629–654..

Pietrafesa, L. J., J. O. Blanton, J. D. Wang, V. Kourafalou, T. N. Lee, and K. A. Bush, 1985: The tidal regime in the South Atlantic Bight. *Oceanography of the Southeastern U.S. Continental Shelf,* L. P. Atkinson, S. W. Menzel, and K. A. Bush, Eds., Coastal and Estuarine Sciences, Vol. 2, Amer. Geophys. Union, 63–76..

Singer, J. J., L. Atkinson, J. O. Blanton, and J. A. Yoder, 1983: Cape Romain and the Charleston Bump: Historical and recent hydrographical observations. *J. Geophys. Res.,* **88,** 4685–4698..

Stern, M., J. A. Whitehead, and B. L. Hua, 1982: The intrusion of a density current along the coast of a rotating fluid. *J. Fluid. Mech.,* **123,** 237–265..

Tebeau, P., and T. N. Lee, 1979: Wind-induced circulation on the Georgia shelf (December 1976–November 1977). University of Miami Tech. Rep. UM RSMAS 79003..

Wang, J. D., V. Kourafalou, and T. N. Lee, 1984: Circulation on the continental shelf of the southeastern United States. Part II: Model development and application to tidal flow. *J. Phys. Oceanogr.,* **14,** 1013–1021.. Find this article online

Weber, A. H., and J. O. Blanton, 1980: Monthly mean wind fields for the South Atlantic Bight. *J. Phys. Oceanogr.,* **14,** 1256–1263.. Find this article online

Figures

Click on thumbnail for full-sized image.

Fig. 1. Continental shelf off the southeastern United States and the locations of ten rivers. The dashed line indicates the domain of the inner shelf model. A cross-shelf section is represented by heavy lines.
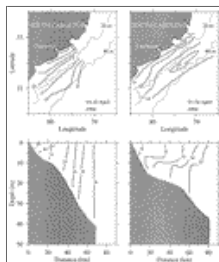
Click on thumbnail for full-sized image.

Fig. 2. Distributions of salinity near the surface and in the vertical near Charleston over the inner shelf of the South Atlantic Bight in Apr 1984. The cross-shelf section was taken near Charleston. The data were digitized directly from figures presented in Paffenhöfer et al. (1994) and replotted. These hydrographic data were taken during the pre-SPREX cruise.
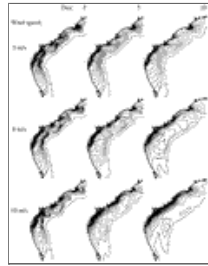
Fig. 3. Schematic of the formation of isolated lens based on the simple wind-induced Ekman theory.
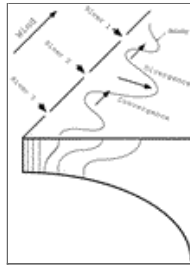
Fig. 4. Schematic of the formation of divergence and convergence zones during an upwelling-favorable wind under conditions of multiple river discharges and M_2 tidal forcing.
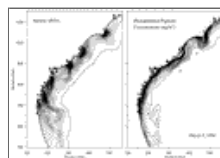
Fig. 5. Time sequences of distributions of the near-surface salinity under different wind conditions for the case with a total river discharge rate of $3R_m$ and tidal forcing.
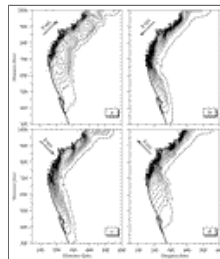
Fig. 6. The tidal-cycle-averaged distributions of the near-surface salinity on the fifth model day after the wind blew for the cases with different directions of wind and the M_2 tidal forcing. The total river discharge rate was $3R_m$.

Fig. 7. Distributions of the surface salinity (left) and CZCS phytoplankton pigment concentration (right) at the end of the 100th day and on 4 March 1984, respectively. The model was forced by an M_2 tidal forcing and a river discharge rate of $5R_m$.
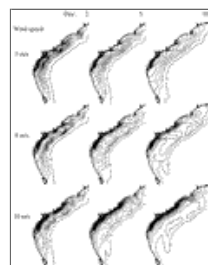
Fig. 8. Time sequences of distributions of near-surface salinity under different wind conditions in the case with a total river discharge rate of $3R_m$ and without tidal forcing. The wind forcing was added into the model at the end of 100th model day.
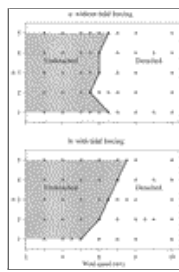
Fig. 9. The relationship of the cross-frontal detachment of low-salinity water with wind speed and total river discharge rate in the cases without and with tidal forcing. Total discharge rate is defined as αR_m: $R_m = 2060$ m^3 s^{-1} is the river discharge rate averaged over a 7 to 74 year dataset and α is an integral number starting from 1. In all cases, the wind forcing was added into the model at the end of the 100th model day.
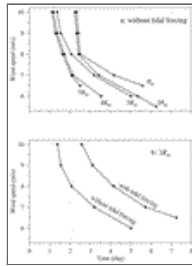
Fig. 10. The dependence of the occurrence time of isolated lenses on total river discharge and wind speed in the case without tidal forcing (a) and a comparison of the occurrence time of lenses between the cases with and without tidal forcing for a given total discharge rate of $3R_m$ (b). In all cases, the wind forcing was added into the model at the end of the 100th model day.
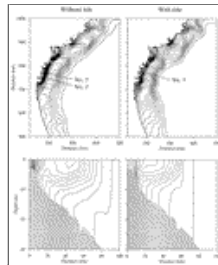
Fig. 11. Comparison of horizontal and vertical distributions of salinity between the cases with and without tidal forcing at the end of the second model day after the wind blew. The model was forced by a river discharge rate of $3R_m$ and a northeastward wind of 8 m s^{-1}. The cross-shelf sections are indicated by solid lines.
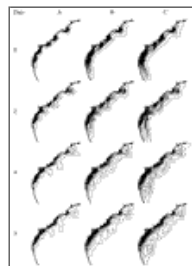
Fig. 12. Distributions of the near-surface salinity at the end of day 0, 2, 4, and 5 for the cases A, B, and C. The model was forced by a river discharge rate of $3R_m$ and tidal forcing. A northeastward wind of 8 m s^{-1} was added into the model on the 10th model day for case A, 50th model day for case B, and 80th model day for case C.
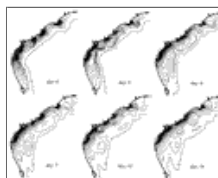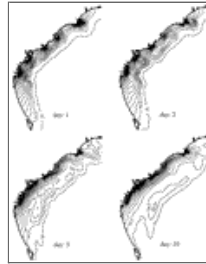
Fig. 13. Distributions of the near-surface salinity at the end of day 0, 2, 4, 7, 12, and 14 for the case with a varying wind. The

model was forced by tidal forcing and a river discharge rate of $3R_m$. A varying northeastward wind was added into the model at the end of the 100th model day.
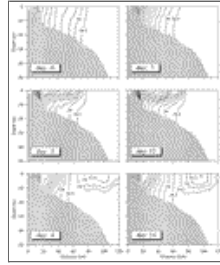
Fig. 14. Distributions of the salinity on a cross-shelf section shown in Fig. 1 ⊙▬ at the end of day 0, 2, 4, 7, 12, and 14 for the case with a varying wind. The model forcings were the same as those given in Fig. 13 ⊙▬.

Fig. 15. Distributions of the near-surface salinity at the end of day 1, 2, 5, and 10 for the case with uniform river discharges. Five major rivers (Cape Fear, Pee Dee, Cooper, Savannah, and Altamaha Rivers) were considered in this experiment, and the river discharge rate at each river was specified as $0.6R_m$. A northeastward wind of 10 m s^{-1} was added into the model at the 100th model day.
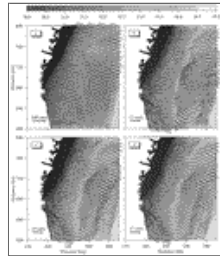
Fig. 16. Evolution of near-surface current vectors on the fifth model day after the wind blew (a) and at the end of day 1, 2, and 5 after the wind ceased [(b), (c), and (d)]. The gray images indicate the distribution of near-surface salinity. The model was forced by tidal forcing and a river discharge rate of $3R_m$.
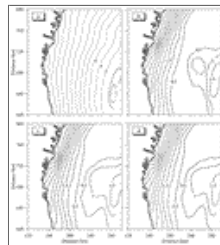
Fig. 17. Evolution of the surface elevation on the fifth model day after the wind blew (a) and at the end of day 1, 2, and 5 after the wind ceased [(b), (c), and (d)]. The model was forced by tidal forcing and a river discharge rate of $3R_m$.
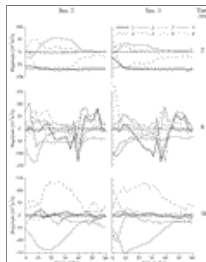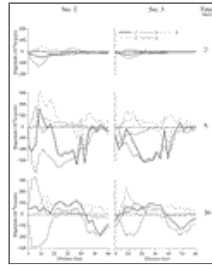
Fig. 18. The cross-shelf distributions of each term in the cross-shelf momentum equation at the 2d, 6th, and 36th hours after the wind began for the case with a total river discharge rate of $3R_m$. The line legend numbers represent the terms in the equation:

$$1: \frac{1}{f}\frac{\partial}{\partial t}\int_{-h_o}^{\zeta} v\, dz; \quad 2: -\int_{-h_o}^{\zeta} u\, dz; \quad 3: \frac{1}{f}\int_{-h_o}^{\zeta}\frac{\partial}{\partial z}\left(K\frac{\partial v}{\partial z}\right)dz; \quad 4: -\frac{g}{f}\int_{-h_o}^{\zeta}\frac{\partial \zeta}{\partial y}\,dz; \quad 5: -\frac{1}{\rho_o f}\int_{-h_o}^{\zeta}\frac{\partial P}{\partial y}\,dz;$$

$$6: -\frac{1}{f}\int_{-h_o}^{\zeta}\frac{\partial uv}{\partial x}\,dz; \quad 7: -\frac{1}{f}\int_{-h_o}^{\zeta}\frac{\partial vv}{\partial y}\,dz; \quad \text{and} \quad 8: -\frac{1}{f}\int_{-h_o}^{\zeta}\frac{\partial wv}{\partial z}\,dz,$$

(Click the equation graphic to enlarge/reduce size)

where u and υ were along- and cross-shelf components of the water velocity. A northeastward wind of 8 m s^{-1} was added into the model at the end of the 100th model day. The locations of sections 2 and 3 were indicated in Fig. 11 ⊙.

Click on thumbnail for full-sized image.

Fig. 19. The cross-shelf distributions of each term in the salt equation at the 2nd, 6th, and 36th hours after the wind began for the case with a total river discharge rate of $3R_m$. The line legend numbers represent the terms in the equation:

$$1: \frac{\partial}{\partial t}\int_{-h_o}^{\zeta} s\, dz; \quad 2: \int_{-h_o}^{\zeta}\frac{\partial}{\partial z}\left(K\frac{\partial s}{\partial z}\right)dz; \quad 3: -\int_{-h_o}^{\zeta}\frac{\partial vs}{\partial y}\,dz; \quad 4: -\int_{-h_o}^{\zeta}\frac{\partial us}{\partial x}\,dz; \quad \text{and} \quad 5: -\int_{-h_o}^{\zeta}\frac{\partial ws}{\partial z}\,dz,$$

where u and υ were along- and cross-shelf components of the water velocity. A northeastward wind of 8 m s^{-1} was added into the model at the end of the 100th model day. The locations of sections 2 and 3 were indicated in Fig. 11 ⊙.

Corresponding author address: Dr. Changsheng Chen, Marine Sciences Building, University of Georgia, Athens, GA 30602-3636.

E-mail: chen@whale.marsci.uga.edu

top ▲